

## PHYSICOCHEMICAL ANALYSIS OF INORGANIC SYSTEMS

# Phase Equilibria in the Tl–TlCl–Te System and Thermodynamic Properties of the Compound $Tl_5Te_2Cl$

D. M. Babanly, Z. S. Aliev, F. Ya. Dhafarli, and M. B. Babanly

Baku State University, Baku, Azerbaijan

e-mail: babanly\_mb@rambler.ru

Received July 7, 2009

**Abstract**—The Tl–Te–Cl system was studied in the Tl–TlCl–Te composition region by differential thermal analysis, X-ray powder diffraction, and emf and microhardness measurements. A series of polythermal sections, an isothermal section at 400 K, and a projection of the liquidus surface of the phase diagram were constructed. The ternary compound  $Tl_5Te_2Cl$  characterized by a wide homogeneity region and incongruent melting by a syntactic reaction at 708 K was shown to exist. This compound was found to crystallize in tetragonal lattice (space group  $I4/mcm$ ) with the parameters  $a = 8.921 \text{ \AA}$ ,  $c = 12.692 \text{ \AA}$ , and  $Z = 4$ . Wide phase separation regions were also found in the system, including a three-phase separation region in the Tl–TlCl– $Tl_2Te$  subsystem. Regions of primary crystallization of phases, and the types and coordinates of in- and monovariant equilibria in the  $T$ – $x$ – $y$  diagram were determined. From emf measurement data, the standard thermodynamic functions of formation and the standard entropy were calculated for the compound  $Tl_5Te_2Cl$ , as follows:  $-\Delta G_{298}^0 = 355.9 \pm 1.1 \text{ kJ/mol}$ ,  $-\Delta H_{298}^0 = 377.1 \pm 5.0 \text{ kJ/mol}$ , and  $S_{298}^0 = 474.1 \pm 6.8 \text{ J/(mol K)}$ .

**DOI:** 10.1134/S0036023611030065

This work continued our physicochemical study of thallium chalcohalides [1–7] and presented new results on phase equilibria and thermodynamic properties of the Tl–Te–Cl system in the Tl–TlCl–Te composition region.

We failed to find any published data on the Tl–Te–Cl system.

Previously [8–12], we investigated the Tl–Te–Cl system over various polythermal sections. In particular [8], we synthesized a new thallium tellurochloride,  $Tl_5Te_2Cl$ , which melts with decomposition by a syntactic reaction at 708 K and crystallizes in the tetragonal lattice (space group  $I4/mcm$ ) with the parameters  $a = 8.921 \text{ \AA}$ ,  $c = 12.692 \text{ \AA}$ , and  $Z = 4$  [8].

The TlCl–Te quasi-binary system [9] is characterized by a wide phase separation region and monotectic equilibrium at 717 K. The eutectic is degenerate near TlCl.

The polythermal sections TlCl–TlTe [10], TlCl– $Tl_2Te_3$ , and Tl– $Tl_2Te_3$ –Tl(TlTe) [11] are non-quasi-binary because of the incongruent melting of one or both of the initial compounds. However, they are stable in the subsolidus region; that is, their alloys consist of two-phase mixtures of the initial phases. In the Tl–TlCl–TlTe system, a wide (to ~20 mol % TlTe) region of Tl–TlCl–Tl-based solid solutions was found [11]. In all of the described sections, there are wide miscibility gaps where liquid separates into two liquid phases and, in the Tl–TlCl–Tl section, even into three liquid phases.

The Tl– $Tl_5Te_2Cl$ –Tl–Te system is also non-quasi-binary and is characterized by the formation of continuous solid solutions [12]. Its interesting specific feature is that the formation of solid solutions is combined with the presence of a wide immiscibility region. The primary crystallization of solid solutions in the composition region 0–65 mol % Tl–Te occurs by a monovariant syntactic reaction.

The boundary constituents Tl–Te and Tl–TlCl of the Tl–TlCl–Te system have been investigated in a number of works. According to the  $T$ – $x$  diagram [13], the compounds  $Tl_5Te_3$ , TlTe, and  $Tl_2Te_3$  form in the Tl–Te system. The first of them melts congruently at 726 K, and the other two melt incongruently at 573 and 511 K, respectively. The compounds  $Tl_5Te_3$  and TlTe crystallize in a tetragonal lattice with the unit cell parameters  $a = 8.929 \text{ \AA}$ ,  $c = 12.620 \text{ \AA}$ ,  $Z = 4$ , space group  $I4/mcm$  [14] and  $a = 12.950 \text{ \AA}$ ,  $c = 6.175 \text{ \AA}$ ,  $Z = 16$  [15] (or  $a = 18.229 \text{ \AA}$ ,  $c = 6.157 \text{ \AA}$ ,  $Z = 32$ , space group  $P4_2/nmc$  [16]), respectively.  $Tl_2Te_3$  has a monoclinic structure with  $a = 17.413 \text{ \AA}$ ,  $b = 6.552 \text{ \AA}$ ,  $c = 7.910 \text{ \AA}$ ,  $\beta = 133.6^\circ$ ,  $Z = 4$ , and space group  $Cc$  [14].

Along with the described compounds, the phase diagram [17] shows the compound  $Tl_2Te$ , which melts congruently at 698 K. It was shown that this compound forms a eutectic with  $Tl_5Te_3$  at 695 K and ~34 mol % Te. These data [17] were later confirmed [18, 19]. However, doubt was cast upon the existence of the compound  $Tl_2Te$  [20] until the publication [21] appeared where, by analyzing 1989 diffraction reflections, it was

established that this compound crystallizes in a monoclinic lattice and is of its own structural type (space group  $C_2/C$ ,  $a = 15.662 \text{ \AA}$ ,  $b = 8.987 \text{ \AA}$ ,  $c = 31.196 \text{ \AA}$ ,  $\beta = 100.7^\circ$ , and  $Z = 4$ ). It was stated [21] that the  $\text{Tl}_2\text{Te}$  crystal lattice contains not only regions characteristic of  $\text{Tl}_5\text{Te}_3$ , but also regions (layers) that comprise only thallium atoms and involve  $\text{Tl}–\text{Tl}$  bonds.

Phase equilibria in the  $\text{Tl}–\text{Cl}$  system were studied in the  $\text{T}–\text{TlCl}_3$  composition region, and a  $T–x$  diagram was constructed [22]. It was found that the compound  $\text{TlCl}$  melts congruently at 703 K, and the  $\text{Tl}–\text{TlCl}$  subsystem is of a monotectic type and is characterized by almost complete immiscibility in the liquid state. The eutectic is degenerate near thallium.

## EXPERIMENTAL

For our studies, we synthesized the compounds  $\text{Tl}_2\text{Te}$ ,  $\text{TlCl}$ , and  $\text{Tl}_5\text{Te}_2\text{Cl}$  and alloys of different compositions in the  $\text{Tl}–\text{TlCl}–\text{Te}$  system.  $\text{Tl}_2\text{Te}$  was synthesized by directly alloying high-purity constituent elements in an evacuated (to  $\sim 10^{-2} \text{ Pa}$ ) quartz ampoule. The alloying temperature was 750 K.

$\text{TlCl}$  was produced according to a published procedure [23]. Initially, metallic thallium was dissolved at  $\sim 350 \text{ K}$  in dilute ( $\sim 7–10 \text{ mol \%}$ ) sulfuric acid to obtain a  $\text{Tl}_2\text{SO}_4$  solution. To a boiling 2%  $\text{Tl}_2\text{SO}_4$  solution, dilute HCl was added until the precipitation was completed. After cooling the mother liquor,  $\text{TlCl}$  was withdrawn, washed with ice distilled water, and dried for a long time in a drying cabinet at 390–400 K.

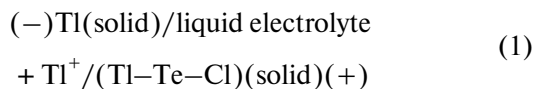
The ternary compound  $\text{Tl}_5\text{Te}_2\text{Cl}$  was produced by alloying the  $\text{TlCl}$  and  $\text{Tl}_2\text{Te}$  obtained as described above in the required ratio in an evacuated quartz ampoule. Because of the syntactic melting of this compound [8], the melts consist of two separating liquid phases. Therefore, heterogeneous mixtures containing  $\text{TlCl}$  and also phases based on  $\text{Tl}_5\text{Te}_2\text{Cl}$  and  $\text{Tl}_2\text{Te}$  crystallize from melts even on slow cooling. Therefore, according to our previous data [8], the completeness of interaction was reached by slow (for  $\sim 5 \text{ h}$ ) cooling to 700 K and treatment at this temperature for  $\sim 300 \text{ h}$ .

The compounds synthesized were identified by differential thermal analysis and X-ray powder diffraction.

By alloying the initial compounds and elemental tellurium and thallium in various ratios in evacuated quartz ampoules, we prepared alloys in the sections  $\text{Tl}_2\text{Te}–[\text{Tl}_2\text{Cl}]$ ,  $\text{Tl}_2\text{Te}–[\text{TlTeCl}]$ , and  $\text{Tl}_5\text{Te}_2\text{Cl}–\text{Te}$  (here and hereinafter, bracketed compounds are heterogeneous alloys taken as “components”) and also a series of additional samples in the  $\text{Tl}–\text{TlCl}–\text{Te}$  composition region. The compositions of the additional samples were chosen based on the phase diagram of the  $\text{Tl}–\text{Te}$  boundary binary system [17] and the data on the previously [8–12] investigated sections in the

$\text{Tl}–\text{TlCl}–\text{Te}$  system. To bring the alloys to equilibrium, they were annealed at temperatures 20–30 K below the solidus temperature for 500–1000 h.

We performed differential thermal analysis with an NTR-72 pyrometer with Chromel/Alumel thermocouples, X-ray powder diffraction with a Philips X’Pert MPD diffractometer ( $\text{CuK}_{\alpha 1}$  radiation), and measurements of microhardness with a PMT-3 microhardness meter (load 20 g) and the emf of concentration circuits of the type



within the temperature range 300–430 K. The electrolyte was a glycerol KCl solution containing  $\sim 0.5 \text{ wt \%}$   $\text{TlCl}$ . The left electrode was made from metallic thallium, which does not directly interact with glycerol [24], and the right electrodes were made from preliminarily synthesized equilibrium alloys in the  $\text{Tl}–\text{TlCl}–\text{Te}$  system in the composition region  $\text{TlCl}–\text{Tl}_2\text{Te}–\text{Te}$ .

The emf was measured by a compensation method with a V7-34A high-resistance digital voltmeter. Circuits of type (1) were produced and the emf was measured according to published procedures [2, 3, 25].

## RESULTS AND DISCUSSION

Processing of the total experimental data set obtained from the above sections and a series of the additional alloys using the  $T–x$  diagrams of the boundary systems  $\text{Tl}–\text{Te}$  [17],  $\text{Tl}–\text{TlCl}$  [22], and  $\text{TlCl}–\text{Te}$  [9] and the previously examined inner sections [8, 10–12], provides a complete self-consistent pattern of phase equilibria in the  $\text{Tl}–\text{TlCl}–\text{Te}$  system (Figs. 1–7, Table 1).

Figure 1 presents the  $T–x$  diagram [8] of the  $\text{TlCl}–\text{Tl}_2\text{Te}$  quasi-binary system together with the results of the measurements of microhardness and the emf of circuits of type (1). In the system the  $\text{Tl}_5\text{Te}_2\text{Cl}$  ternary compound forms, which melts incongruently at 708 K by a syntactic reaction. At the syntactic temperature, the phase separation region extends from  $\sim 7$  to 85 mol %  $\text{Tl}_2\text{Te}$ . A eutectic between  $\text{TlCl}$  and  $\text{Tl}_5\text{Te}_2\text{Cl}$  is at  $\sim 3 \text{ mol \%}$   $\text{Tl}_2\text{Te}$  and 692 K. The compound  $\text{Tl}_5\text{Te}_2\text{Cl}$  forms a series of solid solutions with  $\text{Tl}_2\text{Te}$  which undergoes a morphotropic phase transition from the  $\text{Tl}_5\text{Te}_3$  ( $\delta$  phase) structure to the  $\text{Tl}_2\text{Te}$  ( $\alpha$  phase) structure at  $\sim 90 \text{ mol \%}$   $\text{Tl}_2\text{Te}$  [8].

The X-ray powder diffraction patterns of  $\text{TlCl}–\text{Tl}_2\text{Te}$  alloys from the  $\delta$  phase homogeneity region virtually coincide with the  $\text{Tl}_5\text{Te}_2\text{Cl}$  diffraction pattern and contain no reflection lines representing  $\text{Tl}_2\text{Te}$  (Fig. 2).

The  $\text{Tl}_5\text{Te}_2\text{Cl}$  microhardness remains constant ( $\sim 1340 \text{ MPa}$ ), regardless of the composition in the  $\text{TlCl}–\text{Tl}_5\text{Te}_2\text{Cl}$  region, and monotonically increases to

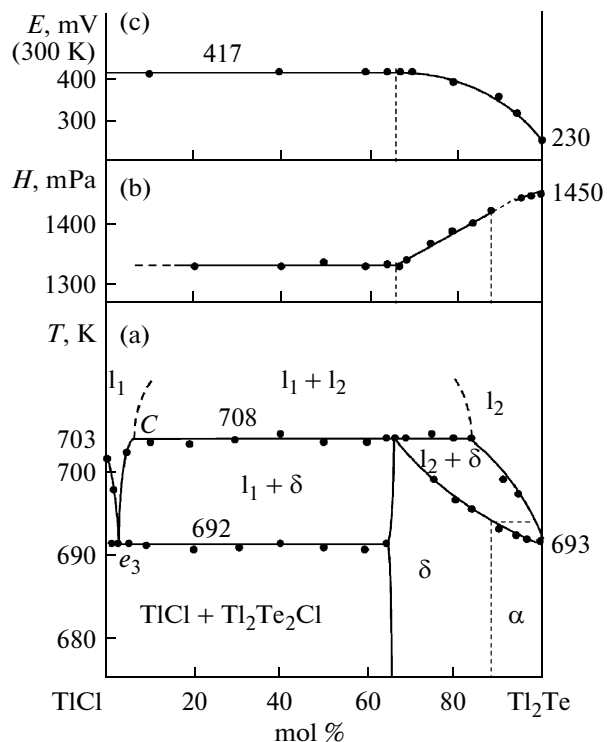


**Fig. 1.** (a)  $T$ - $x$ , (b)  $H$ - $x$ , and (c)  $E$ - $x$  diagrams of the  $\text{TlCl}-\text{Tl}_2\text{Te}$  system.

~1420 MPa within the composition range 66.7–90 mol %  $\text{Tl}_2\text{Te}$ . At high  $\text{Tl}_2\text{Te}$  concentrations, the microhardness slightly decreases from 1450 to ~1420 MPa (Fig. 1b).

The emf continuously increases from 230 mV for the pure  $\text{Tl}_2\text{Te}$  [28] to 417 mV for the stoichiometric-composition phase  $\text{Ti}_5\text{Te}_2\text{Cl}$  and then remains constant. This indicates that each of the alloys within the  $\text{Ti}_5\text{Te}_2\text{Cl}-\text{Tl}_2\text{Te}$  composition region consists of a single phase (Fig. 1c).

**Isothermal section of the  $\text{Tl}-\text{TlCl}-\text{Te}$  system at  $T \leq 500$  K** (Fig. 3) demonstrates the locations of phase regions below the solidus line, in particular, the presence of a wide homogeneity region of  $\text{Ti}_5\text{Te}_2\text{Cl}$ -based alloys ( $\delta$  phase). It is seen that the  $\delta$  phase homogeneity region extends considerably beyond the  $\text{TlCl}-\text{Tl}_2\text{Te}$  section toward an excess of tellurium and has the shape of a wide continuous band for a variable-composition phase based on  $\text{Ti}_5\text{Te}_3$  in the  $\text{Tl}-\text{Te}$  binary system (34.5–38.5 at % Te [17]).

The dominating role in the formation of phase regions in the diagram of solid-phase equilibria is played by  $\text{TlCl}$ , which is the most thermodynamically stable compound in the  $\text{Tl}-\text{Te}-\text{Cl}$  ternary system. This compound is characterized by stable tie-lines to all phases, except  $\text{Ti}_5\text{Te}_3$ , which gives rise to  $\text{Tl} + \delta + \text{TlCl}$ ,  $\text{TlCl} + \text{TlTe} + \delta$ ,  $\text{TlCl} + \text{TlTe} + \text{Tl}_2\text{Te}_3$ , and  $\text{TlCl} + \text{Tl}_2\text{Te}_3 + \text{Te}$  three-phase regions. The compound

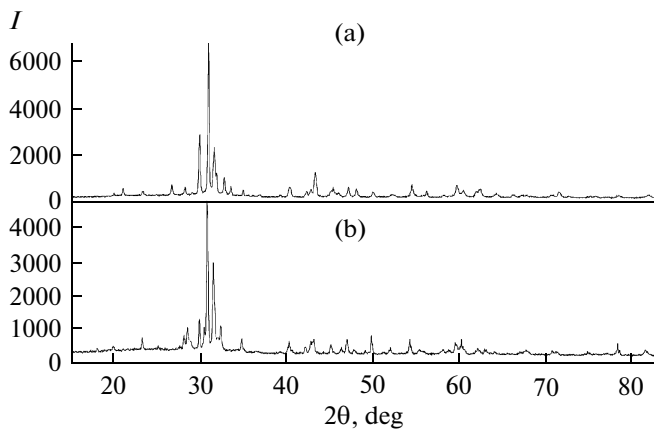


**Fig. 2.** X-ray powder diffraction patterns for (a) the compound  $\text{Ti}_5\text{Te}_2\text{Cl}$  and (b) the alloy containing 85 mol %  $\text{Tl}_2\text{Te}$  in the  $\text{TlCl}-\text{Tl}_2\text{Te}$  section.

$\text{Ti}_5\text{Te}_2\text{Cl}$  and the  $\delta$  phase on its basis are involved in two-phase equilibria with  $\text{TlCl}$  and also with  $\text{TlTe}$  and elemental thallium.

Phase equilibria in complex polythermal sections (Figs. 4–6) are conveniently analyzed together with a projection of the  $T$ - $x$ - $y$  diagram (Fig. 7).

**[ $\text{Tl}_2\text{Cl}$ ]- $\text{Tl}_2\text{Te}$  section** (Fig. 4) contains a wide (~10–80 mol %  $\text{Tl}_2\text{Te}$ ) region where the liquids separates into three liquid phases  $\text{l}_1 + \text{l}_2 + \text{l}_3$ , which is adjacent to  $\text{l}_1 + \text{l}_2$  and  $\text{l}_2 + \text{l}_3$  two-phase fields (where  $\text{l}_1$ ,  $\text{l}_2$ , and  $\text{l}_3$  are liquid solutions based on metallic thallium,  $\text{TlCl}$ , and tellurides, respectively). The horizontal lines at 505 and 575 K represent a polymorphic transition and melting of metallic thallium. The thermal events at 690 and 700 K, respectively, characterize the four-phase monotectic ( $M_1$ ) and syntetic ( $C_T$ ) equilibria (Figs. 4, 7; Table 1). Below the solidus, this section intersects three phase fields:  $\text{Tl}_1 + \alpha$ ,  $\text{Tl}_1 + \delta$ , and  $\text{Tl}_1 + \text{TlCl} + \delta$ .

**$\text{Ti}_5\text{Te}_2\text{Cl}-\text{Te}$  section** (Fig. 5) describes phase equilibria in the  $\text{TlCl}-\text{Tl}_2\text{Te}-\text{Te}$  composition region. In the subsolidus region, this section intersects five phase fields ( $\delta$ ,  $\delta + \text{TlTe}$ ,  $\delta + \text{TlCl} + \text{TlTe}$ ,  $\text{TlCl} + \text{Tl}_2\text{Te}_3 + \text{Te}$ , and  $\text{Tl}_2\text{Te}_3 + \text{TlCl} + \text{Te}$ ), which is in full agreement with the diagram of solid-phase equilibria (Fig. 3). The data on this section allow one to revise the locations of the primary crystallization and immiscibility regions, the run of monovariant equilibrium curves, and the coordinates of a number of nonvariant points of the  $\text{Tl}-\text{TlCl}-\text{Te}$  system (Fig. 7; Table 1).

The liquidus in the  $\text{Ti}_5\text{Te}_2\text{Cl}-\text{Te}$  section consists of three curves corresponding to the primary crystallization of  $\text{TlCl}$ ,  $\delta$  phase, and  $\text{Te}$ . In the composition region 20–100 mol %  $\text{Ti}_5\text{Te}_2\text{Cl}$ , the melt separates into two liquid phases ( $\text{l}_1 + \text{l}_2$ ). From this two-phase melt, in the composition region ~20–85 mol %  $\text{Ti}_5\text{Te}_2\text{Cl}$ ,  $\text{TlCl}$  primarily crystallizes, and in the composition region 85–100 mol %  $\text{Ti}_5\text{Te}_2\text{Cl}$ ,  $\delta$  phase does. In the

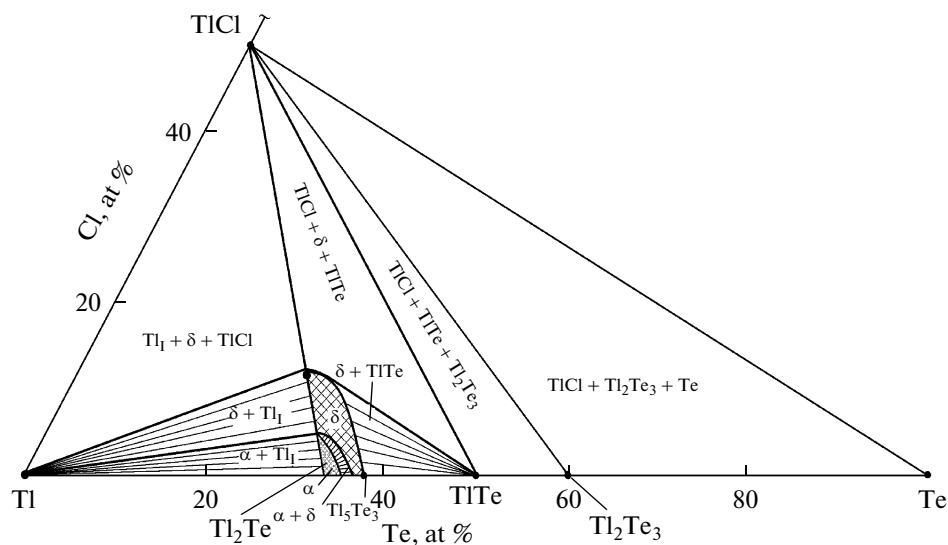


**Fig. 3.** Isothermal section of the phase diagram of the Ti-TiCl-Te system at 300 K.

composition region 0–20 mol %  $\text{Ti}_5\text{Te}_2\text{Cl}$  primarily crystallizes from liquid  $\text{l}_3$  (Fig. 5).

**Tl<sub>2</sub>Te-[TiTeCl] section** (Fig. 6). The pattern of phase equilibria in this section is qualitatively similar to that for the  $\text{Ti}_5\text{Te}_2\text{Cl}$ -Te section. This is because both of the polythermal sections intersect the same phase regions of the  $T$ - $x$ - $y$  diagrams in different directions. The liquidus consists of the curves of primary crystallization of TiCl and the  $\delta$  phase (Fig. 6).

This section, as well as Fig. 5, clearly demonstrates the curves of monovariant ( $M_2P_3$ ,  $P_3P_4$ ,  $P_4E$ , and  $M_3E$ ) and nonvariant ( $M_2$ ,  $P_3$ ,  $P_4$ , and  $E$ ) equilibria (Table 1). In the subsolidus region, this section intersects seven phase fields.

**The liquidus surface of the Ti-TiCl-Te system** (Fig. 7) consists of five fields corresponding to the primary crystallization of TiCl, the  $\delta$  phase, TiTe,  $\text{Ti}_2\text{Te}_3$ , and elemental tellurium. The liquidus surfaces of  $\text{Ti}_2\text{Te}$

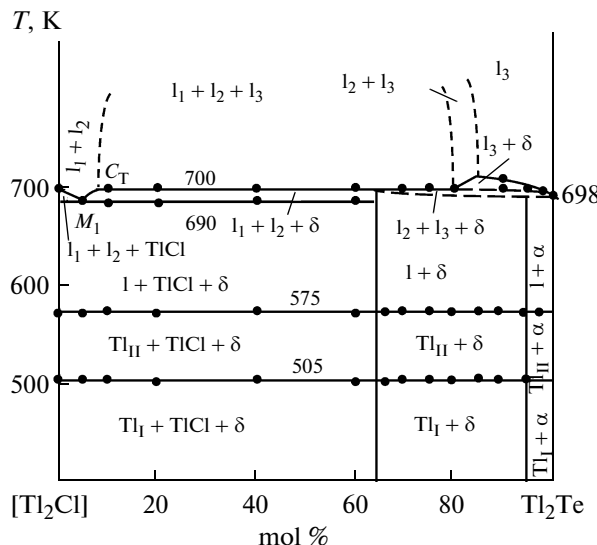


**Fig. 4.** Polythermal section  $[\text{Tl}_2\text{Cl}]-\text{Tl}_2\text{Te}$  of the phase diagram of the Ti-TiCl-Te system.

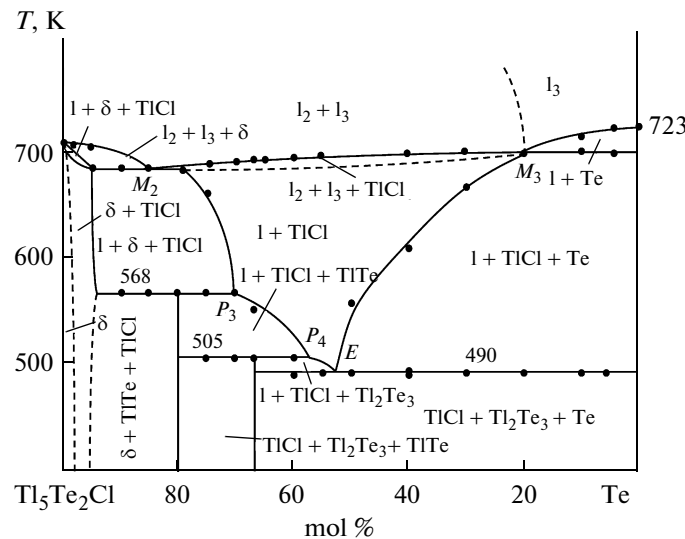


**Fig. 5.** Polythermal section  $\text{Tl}_5\text{Te}_2\text{Cl}-\text{Te}$  of the phase diagram of the Ti-TiCl-Te system.

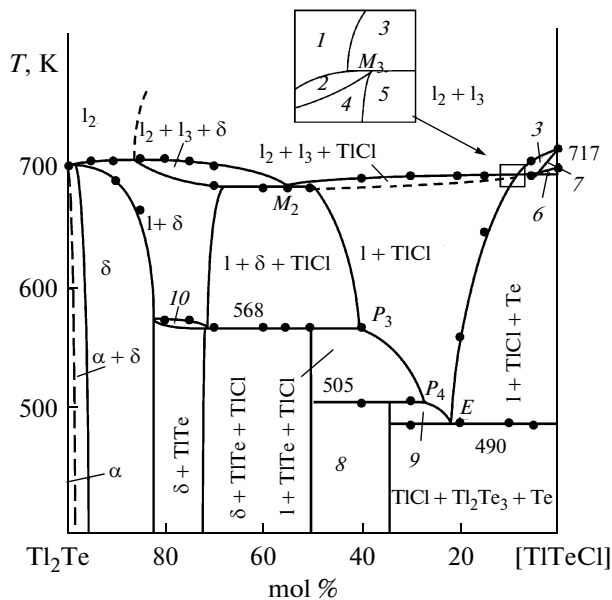


**Fig. 6.** Polythermal section  $\text{Tl}_2\text{Te}-[\text{TlTeCl}]$  of the phase diagram of the  $\text{Tl}-\text{TlCl}-\text{Te}$  system: Phase regions: (1)  $\text{l}_2+\text{l}_3$ , (2)  $\text{l}_2+\text{l}_3+\text{TlCl}$ , (3)  $\text{l}_2+\text{l}_3+\text{Te}$ , (4)  $\text{l}+\text{TlCl}$ , (5)  $\text{l}+\text{TlCl}+\text{Te}$ , (6)  $\text{l}+\text{TlCl}+\text{Te}$ , (7)  $\text{l}+\text{Te}$ , (8)  $\text{TlCl}+\text{TlTe}+\text{Tl}_2\text{Te}_3$ , (9)  $\text{l}+\text{TlCl}+\text{Tl}_2\text{Te}_3$ , and (10)  $\text{l}+\delta+\text{TlTe}$ .

( $\alpha$ ) and elemental thallium are degenerate. Noteworthy is an unusual form of the primary crystallization field of  $\text{TlCl}$  (Fig. 7). On the left along the side of the  $\text{Tl}-\text{TlCl}$  system, this field nearly reaches the thallium vertex of the concentration triangle ( $e_5^*E^*$ ), then significantly narrows ( $E^*M_1^{**}M_1^*e_3^*$ ), and, broadening

again ( $e_3M_2M_2'P_3P_4EM_3'$ ), almost touches the  $\text{Tl}-\text{Te}$  boundary system, after which it narrows again ( $M_3'M_3e_4^*$ ).

A characteristic feature of the  $\text{Tl}-\text{TlCl}-\text{Te}$  system is the presence of wide regions of three-phase melts, namely, those based on metallic thallium ( $\text{l}_1$ );  $\text{TlCl}$

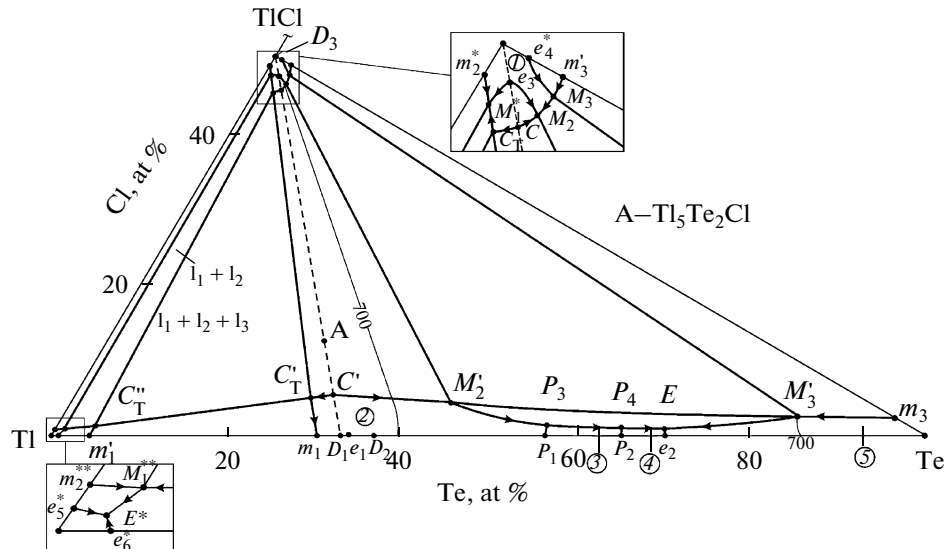


**Fig. 7.** Projection of the liquidus surface of the  $\text{Tl}-\text{TlCl}-\text{Te}$  system. Primary crystallization regions: (1)  $\text{TlCl}$ , (2) the  $\delta$  phase based on  $\text{Tl}_5\text{Te}_2\text{Cl}$ , (3)  $\text{TlTe}$ , (4)  $\text{Tl}_2\text{Te}_3$ , and (5)  $\text{Te}$ . The dashed line is the  $\text{TlCl}-\text{Tl}_2\text{Te}$  quasi-binary section.

**Table 1.** Invariant equilibria in the Tl–TlCl–Te system

Point in Fig. 7	Equilibrium	Composition, at %			T, K
		Tl	Te	Cl	
D <sub>1</sub>	$\text{I}_{D_1} \rightleftharpoons \text{Tl}_2\text{Te}(\alpha)$	66.67	33.33	—	698
D <sub>2</sub>	$\text{I}_{D_2} \rightleftharpoons \text{Tl}_5\text{Te}_3(\delta)$	62.5	37.5	—	723
D <sub>3</sub>	$\text{I}_{D_3} \rightleftharpoons \text{TlCl}$	50	—	50	703
e <sub>1</sub>	$\text{I} \rightleftharpoons \alpha$	66	34	—	695
e <sub>2</sub>	$\text{I} \rightleftharpoons \text{Tl}_2\text{Te}_3 + \text{Te}$	31	69	—	493
e <sub>3</sub>	$\text{I} \rightleftharpoons \text{TlCl} + \delta$	50.5	1.0	48.5	692
e <sub>4</sub> *	$\text{I} \rightleftharpoons \text{TlCl} + \text{Te}$	~50	—	~50	700
e <sub>5</sub> *	$\text{I} \rightleftharpoons \text{Tl}_{\text{II}} + \text{TlCl}$	>99	—	—	575
e <sub>6</sub> *	$\text{I} \rightleftharpoons \text{Tl}_{\text{II}} + \alpha$	>99	—	—	575
E	$\text{I} \rightleftharpoons \text{TlCl} + \text{Tl}_2\text{Te}_3 + \text{Te}$	30.5	68.5	~1	490
P <sub>1</sub>	$\text{I} + \delta \rightleftharpoons \text{TlTe}$	43	57	—	573
P <sub>2</sub>	$\text{I} + \text{TlTe} \rightleftharpoons \text{Tl}_2\text{Te}_3$	35	65	—	508
P <sub>3</sub>	$\text{I} + \delta \rightleftharpoons \text{TlCl} + \text{TlTe}$	43.5	55	~1.5	568
P <sub>4</sub>	$\text{I} + \text{TlTe} \rightleftharpoons \text{TlCl} + \text{Tl}_2\text{Te}_3$	36	63	~1	505
$m_1(m'_1)$	$\text{I}_3 \rightleftharpoons \text{I}_1 + \delta$	69.5(97)	30.5(3)	—	681
$m_2^*(m_2^{**})$	$\text{I}_2 \rightleftharpoons \text{I}_1 + \text{TlCl}$	~51(>99)	—	~49(<1)	700
$m_3(m'_3)$	$\text{I}_2 \rightleftharpoons \text{I}_3 + \text{TlCl}$	2.5(48.5)	95(3)	2.5(48.5)	717
$M_1^*(M_1^{**})$	$\text{I}_2 \rightleftharpoons \text{I}_1 + \text{TlCl} + \delta$	52(>99)	~1	47	690
$M_2(M'_2)$	$\text{I}_2 \rightleftharpoons \text{I}_3 + \text{TlCl} + \delta$	50(53)	3(43)	47(4)	687
$M_3(M'_3)$	$\text{I}_2 \rightleftharpoons \text{I}_3 + \text{TlCl} + \text{Te}$	49(13)	3(85)	48(2)	695
C(C')	$\text{I}_2 + \text{I}_3 \rightleftharpoons \text{Tl}_5\text{Te}_2\text{Cl}(\delta)$	51(65)	2.5(30)	46.5(5)	708
$C_{\text{T}}(C'_{\text{T}}; C''_{\text{T}})$	$\text{I}_2 + \text{I}_3 \rightleftharpoons \text{I}_1 + \delta$	53(68;95)	2(27;4)	46(5;1)	700

Note: The asterisks mark degenerate points; parenthesized are conjugate points and their corresponding compositions.

**Table 2.** Equations of the temperature dependence of the emf in circuits of type (1) at 300–430 K

Phase region in Fig. 3	$E, \text{mV} = a + bT \pm tS_E(T)$
$\text{Tl}_5\text{Te}_2\text{Cl} + \text{TlCl} + \text{TlTe}$	$420.4 + 0.0124T \pm 2[2.379/22 + 7.5 \times 10^{-5}(T - 360.4)^2]^{1/2}$
$\text{TlCl} + \text{TlTe} + \text{Tl}_2\text{Te}_3$	$431.6 + 0.020T \pm 2[3.44/22 + 1.5 \times 10^{-4}(T - 361.8)^2]^{1/2}$
$\text{TlCl} + \text{Tl}_2\text{Te}_3 + \text{Te}$	$436.8 + 0.079T \pm 2[2.55/22 + 8.2 \times 10^{-5}(T - 361.8)^2]^{1/2}$

( $\text{I}_2$ ); and  $\delta$  phase, tellurides, and elemental tellurium ( $\text{I}_3$ ). These regions occupy more than 90% of the area of the concentration triangle of the Tl–TlCl–Te system. For the system, there is a wide field of three-phase melts:  $C_{\text{T}}C'_{\text{T}}C''_{\text{T}}$  (Fig. 7), which is surrounded by the corresponding two-phase melt fields. The triangle  $C_{\text{T}}C'_{\text{T}}C''_{\text{T}}$  is characterized by invariant syntectic equilib-

rium  $\text{I}_2 + \text{I}_3 \rightleftharpoons \text{I}_1 + \delta$  at 700 K (Table 1). The formation of the three-phase separation field is due to the presence of three wide separation regions ( $m_1m'_1$ ,  $m_2^*m_2^{**}$ , and  $CC'$ ) along all of the sides of the concentration triangle of the Tl–TlCl–Tl<sub>2</sub>Te subsystem.

The immiscibility regions  $CC'$  and  $m_3m'_3$  in the TlCl–Tl<sub>2</sub>Te and TlCl–Te quasi-binary sections extend

**Table 3.** Standard integral thermodynamic functions for the compounds  $\text{Ti}_5\text{Te}_2\text{Cl}$ ,  $\text{TiCl}$ , and  $\text{TiTe}$ 

Compound	$-\Delta G_{298}^0$	$-\Delta H_{298}^0$	$S_{298}^0$
	kJ/mol	J/(mol K)	
$\text{TiCl}$ [29]	$185.0 \pm 0.8$	$208.3 \pm 3.0$	$111.5 \pm 0.2$
$\text{TiTe}$ [28]	$44.5 \pm 0.4$	$43.9 \pm 0.5$	$115.9 \pm 1.6$
$\text{Ti}_5\text{Te}_2\text{Cl}$	$355.9 \pm 1.1$	$377.1 \pm 5.0$	$474.1 \pm 6.8$

deep into the concentration triangle of the  $\text{TiCl}-\text{Ti}_2\text{Te}-\text{Te}$  subsystem and form a wide continuous band of two-phase melts:  $\text{l}_2 + \text{l}_3$ . The eutectic curve originating at point  $e_3$  intersects this two-phase region. As a result, the horizontal line  $M_2M'_2$  characterized by invariant monotectic equilibrium forms (Table 1).

The phases in the immiscibility regions crystallize by various monotectic and syntectic reactions (Fig. 7, Table 1). Table 1 presents the types of invariant equilibria and the coordinates of the corresponding points for the  $\text{Ti}-\text{TiCl}-\text{Te}$  system.

The emf measurements not only confirmed the solid-phase equilibrium diagram for the  $\text{TiCl}-\text{Ti}_2\text{Te}-\text{Te}$  subsystem but also allowed us to determine the thermodynamic functions of the compound  $\text{Ti}_5\text{Te}_2\text{Cl}$ . Because the temperature dependence of the emf was linear, these data were processed by the least-squares method [26]. The results are presented in Table 2 as equations of the type  $E = a + bT \pm tS_E(T)$  [27]. We found that, within each of the three-phase regions ( $\text{TiCl}-\text{TiTe}-\delta$ ,  $\text{TiCl}-\text{TiTe}-\text{Ti}_2\text{Te}_3$ , and  $\text{TiCl}-\text{Ti}_2\text{Te}_3-\text{Te}$ ), the emf is independent of the bulk composition of the alloy. In the last two of the three regions, the emf values coincide to an accuracy of  $\pm 3$  mV with the data [28] for pure  $\text{TiTe}$  and  $\text{Ti}_2\text{Te}_3$ . This, first, indicates the reversibility of circuits of type (1) and, second, confirms our results on the insignificance of the  $\text{TiTe}$  and  $\text{Ti}_2\text{Te}_3$  homogeneity regions in the  $\text{Ti}-\text{TiCl}-\text{Te}$  system.

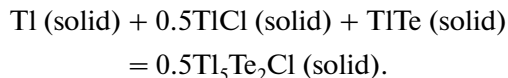
We used known thermodynamic relations from the temperature dependence of the emf in the three-phase region  $\text{TiCl}-\text{Ti}_5\text{Te}_2\text{Cl}-\text{TiTe}$  (Table 2) to calculate the relative partial molar functions of thallium at 298 K:

$$\overline{\Delta G_{\text{Ti}}} = -(40.92 \pm 0.12) \text{ kJ/mol},$$

$$\overline{\Delta H_{\text{Ti}}} = -(40.56 \pm 0.61) \text{ kJ/mol},$$

$$\overline{\Delta S_{\text{Ti}}} = (1.20 \pm 1.67) \text{ J/(mol K)}.$$

According to the solid-phase equilibrium diagram (Fig. 3), these functions are thermodynamic characteristics of the following potential-forming reaction [25]:



Thus, the standard thermodynamic functions of formation and the standard entropy for the compound  $\text{Ti}_5\text{Te}_2\text{Cl}$  can be calculated from

$$\begin{aligned} \Delta Z^0(\text{Ti}_5\text{Te}_2\text{Cl}) \\ = 2\overline{\Delta Z_{\text{Ti}}} + \Delta Z^0(\text{TiCl}) + 2\Delta Z^0(\text{TiTe}), \end{aligned}$$

where  $\Delta Z$  is  $\Delta G$ ,  $\Delta H$ , or  $\Delta S$ , and

$$\begin{aligned} S^0(\text{Ti}_5\text{Te}_2\text{Cl}) \\ = 2\overline{\Delta S_{\text{Ti}}} + 2S^0(\text{Ti}) + S^0(\text{TiCl}) + 2S^0(\text{TiTe}) \end{aligned}$$

respectively. In the calculations we used both our own data on  $\overline{\Delta Z_{\text{Ti}}}$ , and published data on the corresponding thermodynamic characteristics of  $\text{TiCl}$  [29] and  $\text{TiTe}$  [28] (Table 3) and the standard entropy of elemental thallium. Table 3 presents the calculation results. The errors were found by the error accumulation method,

## REFERENCES

1. M. B. Babanly, G. M. Guseinov, D. M. Babanly, and F. M. Sadygov, *Zh. Neorg. Khim.* **51** (5), 876 (2006) [Russ. J. Inorg. Chem. **51** (5), 805 (2006)].
2. D. M. Babanly, Yu. A. Yusibov, and M. B. Babanly, *Zh. Neorg. Khim.* **52** (5), 819 (2007) [Russ. J. Inorg. Chem. **52** (5), 753 (2007)].
3. D. M. Babanly, Yu. A. Yusibov, and M. B. Babanly, *Zh. Neorg. Khim.* **52** (5), 827 (2007) [Russ. J. Inorg. Chem. **52** (5), 761 (2007)].
4. R. A. Alieva, I. M. Babanly, D. M. Babanly, and I. I. Aliev, *Vestn. BGU, Ser.: Estestv. Nauk*, No. 4, 83 (2004).
5. R. A. Alieva, I. M. Babanly, D. M. Babanly, and I. I. Aliev, *Khim. Problemy* (Baku), No. 4, 83 (2004).
6. M. B. Babanly, G. M. Guseinov, D. M. Babanly, and F. M. Sadygov, *Khim. Problemy* (Baku), No. 2, 141 (2007).
7. D. M. Babanly and M. B. Babanly, *Zh. Neorg. Khim.* **55** (10), 1725 (2010) [Russ. J. Inorg. Chem. **55** (10), 1620 (2010)].
8. D. M. Babanly, A. A. Nadzhafova, M. I. Chiragov, and M. B. Babanly, *Khim. Problemy* (Baku), No. 2, 149 (2005).
9. D. M. Babanly, I. M. Babanly, N. A. Rzaeva, and I. I. Aliev, *Proceedings of IX Republican Scientific Conference "Physicochemical Analysis and Inorganic Materials Science"* (Baku, 2004), p. 49 [in Russian].
10. D. M. Babanly, Yu. A. Yusibov, and I. I. Aliev, *Khim. Problemy* (Baku), No. 1, 183 (2006).
11. D. M. Babanly and Yu. A. Yusibov, *Khim. Problemy* (Baku), No. 4, 661 (2006).
12. D. M. Babanly, I. I. Aliev, Yu. A. Yusibov, and M. I. Chiragov, *Azerb. Khim. Zh.*, No. 1, 151 (2007).
13. N. Kh. Abrikosov and L. E. Shelimova, *Chalcogenide Semiconductors and Their Based Alloys* (Nauka, Moscow, 1975) [in Russian].
14. S. Bhan and K. Shubert, *J. Less-Common Met.* **20** (3), 229 (1970).

15. A. Rabenay, A. Stegherr, and P. Eckerlin, *Z. Metallkunde* **51** (5), 295 (1960).
16. K. Stöwe, *J. Solid State Chem.* **149** (1), 123 (2000).
17. M. M. Asadov, M. B. Babanly, and A. A. Kuliev, *Izv. Akad. Nauk SSSR, Ser. Neorg. Mater.* **13** (8), 1407 (1977).
18. H. Said and R. Castanet, *Z. Metallkunde* **69** (3), 281 (1978).
19. M. C. Record, Y. Feutelais, and H. L. Lukas, *Z. Metallkunde* **88**, 45 (1997).
20. H. Okamoto, *J. Phase Equilibr.* **15** (1), 131 (1994).
21. R. Cerny, J. Joubert, Y. Filinchuk, and Y. Feutelais, *Acta Crystallogr., Sect. C: Cryst. Struct. Commun.* **58** (5), 163 (2002).
22. *Binary Alloy Phase Diagrams*, Ed. by T. B. Massalski (ASM, Materials Park, Ohio, 1990).
23. *Handbuch der präparativen anorganischen Chemie*, Ed. by G. Brauer (Enke, Stuttgart, 1978; Mir, Moscow, 1985).
24. N. Ya. Turova and A. V. Novoselova, *Usp. Khim.* **34** (3), 385 (1956).
25. M. B. Babanly, Yu. A. Yusibov, and V. T. Abishev, *EMF Measurements in the Thermodynamics of Compound Semiconductors* (BGU, Baku, 1992) [in Russian].
26. K. Doerffel, *Statistik in der analytische Chemie* (Deutsche Verlag für Grundstoffindustrie, Leipzig, 1990; Mir, Moscow, 1994).
27. A. N. Kornilov, L. B. Stepina, and V. A. Sokolov, *Zh. Fiz. Khim.* **46** (11), 2974 (1972).
28. V. P. Vasil'ev, A. V. Nikol'skaya, Ya. I. Gerasimov, and A. F. Kuznetsov, *Izv. Akad. Nauk SSSR, Ser. Neorg. Mater.*
29. Kubaschewski, C. B. Alcock, and P. Spenser, *Materials Thermochemistry* (Pergamon, New York, 1993).